Performance evaluation and segmentation for synthetic aperture radar image using mixture multiscale autoregressive model and bootstrap technique

Haixia Xu (徐海霞)[1,2*], Xianbin Wen (温显斌)[1,2], Yongliao Zou (邹永廖)[3], and Yongchun Zheng (郑永春)[3]

[1] *Tianjin Key Laboratory of Intelligence Computing and Novel Software Technology, Tianjin University of Technology, Tianjin 300384, China*

[2] *Key Laboratory of Computer Vision and System of Ministry of Education, Tianjin University of Technology, Tianjin 300384, China*

[3] *National Astronomical Observatories, Chinese Academy of Sciences, Beijing 100012, China*

[*] *Corresponding author: xuhaixia_xhx@163.com*

Received December 14, 2011; accepted January 18, 2012; posted online April 27, 2012

An unsupervised segmentation and its performance evaluation technique are proposed for synthetic aperture radar (SAR) image based on the mixture multiscale autoregressive (MMAR) model and the bootstrap method. The segmentation-evaluation techniques consist of detecting the number of image regains, estimating MMAR parameters by using bootstrap stochastic annealing expectation-maximization (BSAEM) algorithm, and classifying pixels into region by using Bayesian classifier. Experimental results demonstrate that the evaluation operation is robust, and the proposed segmentation method is superior to the traditional single resolution techniques, and considerably reduces the computing time over the EM algorithm.

OCIS codes: 100.0100, 280.6730.

doi: 10.3788/COL201210.S11005.

Synthetic aperture radar (SAR) imaging systems have been widely used in the past several years for remote sensing applications. One of the main advantages of these systems is the ability to operate at any time of day, in any weather conditions, and to improve the image resolution for a given aperture size. However, coherent active imaging has the drawback of leading to images that are degraded by speckle noise which makes the images grainy and deteriorate the image processing performances. The low-level step of image segmentation, i.e., the decomposition of the image in a tessellation of uniform areas, is a crucial point of SAR images processing.

Numerous segmentation methods have been proposed in the research literature, e.g., thresholding methods[1,2], clustering methods[3,4], edge-based methods[5], region splitting and merging methods[6,7], and multi-resolution techniques[8−16]. Recently, to characterize and exploit the scale-to-scale statistical variations in SAR image duo to radar speckle[11], various multiscale stochastic models have been developed and used for segmentation of SAR image. Basserille *et al.* proposed a multiscale autoregressive model for signal and image processing[15]. Fosgate *et al.*, Irving *et al.*, and Kim *et al.* build the models representative of each category of terrain of interest SAR image and employ them in directing decisions on pixel classification, segmentation behavior[11−13]. Comer *et al.* proposed a segmentation algorithm based on the multiresolution Gaussian autoregressive model for the observed image pyramid[17]. The algorithm used a multiresolution Gaussian autoregressive model for the pyramid representation of observed image, and assumes a multiscale Markov random field model for the class label pyramid. Wen *et al.* proposed a mixture multiscale autoregressive (MMAR) model for the segmentation of SAR image[18], and gave Bayesian segmentation for SAR image based on the MMAR model, which parameters are estimated by using expectation-maximization (EM) algorithm. MMAR model provides a powerful multiscale and semi-parameter framework for describing unknown distributional shape of complex random field that evolve in scale. However, the EM algorithm has the problem that the solution converges to a local optimal due to the dependence of the initial state of parameters in the posterior distribution. On the other hand, in the statistical segmentation, the time increases with the size of training data set. In most of the real-world application, the size of the training data is very large. As a result, the time required by segmentation could be prohibitively large. Finally, how good are these techniques in term of their detection and classification performances is not known.

This letter addresses SAR image segmentation and performance evaluation based Bootstrap technology and mutiscale stochastic model on the tree without supervision. Firstly, the estimation algorithm by using Bootstrap technique[19], namely, bootstrap stochastic annealing EM (BSAEM) algorithm, is proposed, which algorithm improves the EM algorithm by adding an optimal Bootstrap sample selection and decorrelation step to the blind approach, and would converge more rapidly to the good solution then the classical EM algorithm. Secondly, the detection performance based on the MMAR model is discussed, where the statistical probabilities of over-detection and under-detection of the number of image regions are defined, and the corresponding formula in terms of the model parameters and the image quality are derived. Thirdly, we define misclassification probability for the Bayesian classifier and give a simple formula to evaluate segmentation errors based on the parameter estimates and classified data. Finally, tests have been conducted on three real SAR images for evaluating de-

tection and classification performance.

The starting point for our model development is a multiscale sequence $\mathbf{X}_L, \mathbf{X}_{L-1}, \cdots, \mathbf{X}_0$ of SAR image, where $\mathbf{X}_L$ and $\mathbf{X}_0$ correspond to the coarsest and finest resolution images, respectively. The resolution varies dyadically between images at successive scales. More precisely, we assume that the finest scale image $\mathbf{X}_0$ has a resolution of $\delta \times \delta$ and consists of an $N \times N$ array of pixels (with $N = 2^M$ for some M). Hence, each coarser resolution image $\mathbf{X}_m$ has $2^{-m}N \times 2^{-m}N$ pixels and resolution $2^m\delta \times 2^m\delta$. Each pixel $X_m(k,l)$ is obtained by taking the coherent sum of complex fine-scale imagery over $2^m \times 2^m$ blocks, performing log-detection (computing 20 times the log-magnitude), and correcting for zero frequency gain variations by subtracting the mean value. According, each pixel in image $\mathbf{X}_m$ corresponds to four "child" pixels in image $\mathbf{X}_{m-1}$. This indicates that quadtree is natural for the mapping. Each node s on the tree is associated with one of the pixels $X_m(k,l)$ corresponding to pixel (k,l) of SAR image $\mathbf{X}_m$.

As an example, Fig. 1 illustrates a multiscale sequence of three SAR images, together with the quadtree mapping. We notice that the quadtree is different from the quadtree in wavelet analysis for image processing. One different is that there is some spatial connectivity between nodes at the same level in the quadtree of this letter, however, there is no spatial connectivity in the quadtree of wavelet for image analysis. We use the notation $X(s)$ to indicate the pixel mapped to node s. The scale of node s is denoted by $m(s)$.

For complex SAR image, we define the MMAR model of SAR imagery as

$$F[X(s)|\mathbf{\Theta}, \mathbf{X}_s] = \sum_{k=1}^{K} \pi_k \Phi \left(\frac{X(s) - a_{k,0} - a_{k,1}X(s\bar{\gamma}) - \cdots - a_{k,p_k}(s\bar{\gamma}^{p_k})}{\sigma_k} \right), \quad (1)$$

or

$$f[X(s)|\mathbf{\Theta}, \mathbf{X}_s] = \sum_{k=1}^{K} \frac{\pi_k}{\sigma_k} \varphi \left(\frac{X(s) - a_{k,0} - a_{k,1}X(s\bar{\gamma}) - \cdots - a_{k,p_k}(s\bar{\gamma}^{p_k})}{\sigma_k} \right), \quad (2)$$

where $\pi_1, \pi_2, \cdots, \pi_K$ are the mixing proportions with $\sum_{k=1}^{K} \pi_k = 1$, $\pi_k > 0$, $\mathbf{\Theta} = (\pi_1, \cdots, \pi_K, \boldsymbol{\theta})$, $\boldsymbol{\theta} = (\boldsymbol{\theta}_1, \cdots, \boldsymbol{\theta}_K)$, $\boldsymbol{\theta}_k = (a_{k,0}, \cdots, a_{k,p_k}, \sigma_k)$, $a_{k,0}, \cdots, a_{k,p_k}$ are the k class autoregressive coefficients, σ_k^2 is the k class variance. F is the distribution function, and f is probability density function. K is the number of classes, $\mathbf{X}_s$ is the set of $X(s\bar{\gamma}), \cdots, X(s\bar{\gamma}^p)$ $(p = \max_k p_k)$, and $\Phi(.)$ is the standard normal distribution function. $\varphi(.)$ is the probability density function of a standard normal distribution. We denote this model by MMAR $(K, p_1, \cdots, p_K)$. It is clear that MMAR $(K, p_1, \cdots, p_K)$ is actually a mixture of K Gaussian MAR models, and MAR is a special case of MMAR when $K = 1$.

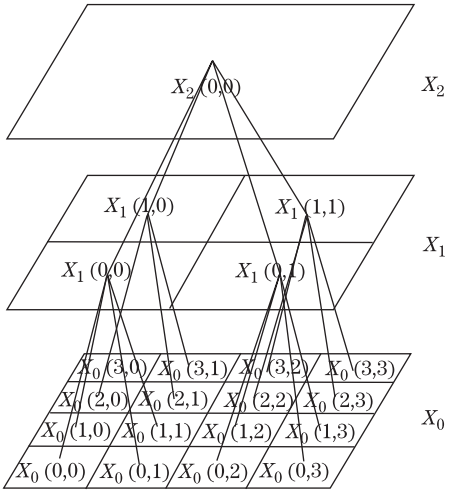

Fig. 1. Sequence of three multiresolution SAR images mapped onto a quadtree.

Given a SAR image with statistical MMAR distribution (1) or (2), Bootstrap samples, denoted by $X^*(s)$, are drawn from mscale SAR image. For Bootstrap samples, the log-likelihood of the maximization likelihood (ML) estimate of the MMAR parameters is given by

$$\mathrm{L}(K, \mathbf{\Theta}) = \sum_{N, \{s|m(s)=m\}} \ell_s = \sum_{N, \{s|m(s)=m\}} \left\{ \sum_{k=1}^{K} \mathbf{Z}_{s,k} \log(\pi_k) - \sum_{k=1}^{K} \mathbf{Z}_{s,k} \log(\sigma_k) - \sum_{k=1}^{K} \frac{\mathbf{Z}_{s,k} e_{ks}^{*2}}{2\sigma_k^2} \right\}, \quad (3)$$

where $e_{ks}^* = X^*(s) - a_{k,0} - a_{k,1}X^*(s\bar{\gamma}) - \cdots - a_{k,p}X^*(s\bar{\gamma}^p)$, $X^*(s\bar{\gamma})$ is parent of $X^*(s)$, N is the number of pixels in the Bootstrap samples. $\mathbf{Z}_s$ is a K-dimensional vector with component $k = 1$ if $X(s)$ comes from the kth component of the conditional distribution function and otherwise $k = 0$.

The iterative BSAEM algorithm for estimating parameters by Eq. (3) consists of an E-step, a stochastic step (S-step), an annealing step (A-step) and an M-step, which can be described below:

E-step: Suppose that $\mathbf{\Theta}$ is known. The missing data $\mathbf{Z}$ are then replaced by their conditional expectations, conditional on the parameters and on the data $\mathbf{X}$. In this case, the conditional expectation of the kth component of $\mathbf{Z}_s$ is just the conditional probability that the data $X(s)$ comes from the kth component of the MMAR. Let $\tau_{s,k}$ be the conditional expectation of the kth component of $\mathbf{Z}_s$. Then, the E-step equations are

$$\tau_{s,k} = \frac{\pi_k(1/\sigma_k)\varphi(e_{ks}^*/\sigma_k)}{\sum_{k=1}^{K} \pi_k(1/\sigma_k)\varphi(e_{ks}^*/\sigma_k)}, \quad k = 1, \cdots, K, \quad (4)$$

S-Step: Then, construct a Bernouilli random variable $z_{s,k}$ of parameter $\tau_{s,k}$.

A-Step: From $z_{s,k}$ and $\tau_{s,k}$, one can construct another random variable

$$w_{s,k} = \tau_{s,k} + h_n(z_{s,k} - \tau_{s,k}), \quad (5)$$

where h_n is a given sequence which slowly decreases to zero during iterations.

M-Step: In this step, $w_{s,k}$ is considered artificially as the a posterior probability of $X^*(s)$, so that, at next iteration, we have

$$\hat{\pi}_k = \frac{\sum\limits_{\{s|m(s)=0\}} w_{s,k}}{N}, \quad k = 1, \cdots, K, \tag{6}$$

$$\hat{\sigma}_k^2 = \frac{\sum\limits_{\{s|m(s)=m\}} w_{s,k}[X^*(s) - \hat{a}_{k,0} - \hat{a}_{k,1}X^*(s\bar{\gamma}) - \cdots - \hat{a}_{k,p}X^*(s\bar{\gamma}^p)]^2}{\sum\limits_{\{s|m(s)=m\}} w_{s,k}}, \quad k = 1, \cdots, K, \tag{7}$$

where $(\hat{a}_{k,0}, \hat{a}_{k,1}, \cdots, \hat{a}_{k,p})$ satisfy the system of equations.

$$\sum_{\{s|m(s)=m\}} w_{s,k}X^*(s)\mu[X^*(s), i] = \sum_{j=1}^{p} \hat{a}_{k,j} \sum_{\{s|m(s)=m\}} \cdot w_{s,k}\mu(X^*(s), j)\mu(X^*(s), i), \quad i = 1, \cdots, p, \tag{8}$$

where $\mu[X^*(s), i] = 1$ for $i = 0$ and $\mu(X^*(s), i) = X^*[s\bar{\gamma}^i]$ for $i > 0$.

The estimates of the parameters are then obtained by iterating the four steps until convergence. Parameters K, p_k can be selected by Bayesian information criterion (BIC). That is

$$I(K) = -\ln[\mathrm{L}(K, \mathbf{\Theta})] + \ln(N - p_{\max}) \cdot \left(3K - 1 + \sum_{j=1}^{K} p_j\right). \tag{9}$$

Assume that the orders p_k $(k = 1, \cdots, K)$ of the model are known. Let K_0 and K_1 denote the real number and detected number by the BIC of SAR image regions, respectively, then the probabilities of over-detected and under-detected of the number of SAR image regions can be defined by

$$P_{\text{over}} = P\{K_1 - K_0 > 0\} = P\{I(K_1) < I(K_0)\}, \tag{10}$$

and

$$P_{\text{under}} = P\{K_1 - K_0 < 0\} = P\{\mathrm{I}(K_1) < \mathrm{I}(K_0)\}, \tag{11}$$

and the error-detected probability can be defined

$$P_{\text{error}} = P\{K_1 - K_0 \neq 0\}, \tag{12}$$

From Eqs. (10) and (11), Eq. (12) can be written as

$$P_{\text{error}} = P\{I(K_1) < I(K_0)\}, \tag{13}$$

Applying Eq. (9) to $I(K_0)$ and $I(K_1)$ in Eq. (13), then

$$P\{\ln[L(K_0, \mathbf{\Theta})] - \ln[L(K_1, \mathbf{\Theta})] < 3\ln(N - p_{\max})(K_0 - K_1)\}, \tag{14}$$

In Eq. (2), when $\hat{\sigma}_j^2 > 1/2\pi$, $0 < \mathrm{f}(\mathrm{x}(s)|\mathbf{\Theta}, X_{\mathrm{s}}) < 1$. From $\ln w \approx w - 1$, $(0 < w \leqslant 2)$, then

$$\ln[L(K, \mathbf{\Theta})] = \sum_{m(s)=\mathrm{l}} \ln[f(X(s)|\mathbf{\Theta}, X_{\mathrm{s}})] \approx \sum_{m(s)=\mathrm{l}} f(X(s)|\mathbf{\Theta}, X_{\mathrm{s}}) - N. \tag{15}$$

Assuming that $\pi_j = 1/K$, and $\sigma_j^2 = \sigma^2$, $j = 1, 2, \cdots, K$, Eq. (15) becomes

$$\ln[\mathrm{L}(K, \mathbf{\Theta})] = \frac{1}{\sqrt{2\pi}K\sigma} \sum_{m(s)=1} \sum_{j=1}^{K} \exp\left\{-\frac{e_j^2(s)}{2\sigma^2}\right\} - N. \tag{16}$$

Pixel $X(s)$ is a sample from the MMAR. After classification, $X(s)$ belong to one and only one image region, say $\mathbf{G}_k$. Let $n_0 = 0$, $n_K = N$. Without loss of generality, assume $\{X(s_{n_{k-1}+1}), \cdots, X(s_{n_k})\} \in \mathbf{G}_k$, $(k = 1, \cdots, K)$. By using $\exp(-\frac{1}{2}w) \approx 1 - \frac{1}{2}w$, we have

$$\begin{aligned}\ln[L(K, \mathbf{\Theta})] &= \frac{1}{\sqrt{2\pi}K\sigma} \sum_{k=1}^{K} \sum_{j=n_{k-1}+1}^{n_k} \exp\left\{-\frac{e_k^2(s_j)}{2\sigma^2}\right\} - N \\ &\approx \frac{1}{\sqrt{2\pi}K\sigma} \sum_{k=1}^{K} \sum_{j=n_{k-1}+1}^{n_k} \left(1 - \frac{e_k^2(s_j)}{2\sigma^2}\right) - N \\ &\approx \frac{1}{\sqrt{2\pi}K\sigma} \left[N - \frac{1}{2} \sum_{k=1}^{K} \sum_{j=n_{k-1}+1}^{n_k} \frac{e_k^2(s_j)}{2\sigma^2}\right] - N.\end{aligned} \tag{17}$$

Define

$$\sum_{k=1}^{K} \sum_{j=n_{k-1}+1}^{n_k} \frac{e_k^2(s_j)}{2\sigma^2} = Y_K, \tag{18}$$

Eq. (17) becomes

$$\ln[L(K, \mathbf{\Theta})] \approx \frac{1}{\sqrt{2\pi}K\sigma} \left[N - \frac{1}{2}Y_K\right] - N. \tag{19}$$

Because $\sum_{j=n_{k-1}+1}^{n_k} e_k^2(s_j)/\sigma^2$ has a χ^2 distribution with degree of freedom $(n_k - n_{k-1} - p_k - 1)$, Y_K has a χ^2 distribution with degree of freedom $(N - K - \sum_{j=1}^{K} p_j)$.

Applying Eq. (19) to $L(K_0, \mathbf{\Theta_0})$ and $L(K_1, \mathbf{\Theta_1})$ in Eq. (14) with $\mathbf{\Theta} = \mathbf{\Theta_0}$ (when $K = K_0$) and $\mathbf{\Theta} = \mathbf{\Theta_1}$ (when $K = K_1$), we have

$$P_{\text{error}} = P\left\{\frac{1}{K_1\sigma_1}Y_{K_1} - \frac{1}{K_0\sigma_0}Y_{K_0} < 6\sqrt{2\pi}\ln(N - p_{\max})(K_0 - K_1) + 2N\left(\frac{1}{K_1\sigma_1} - \frac{1}{K_0\sigma_0}\right)\right\}. \tag{20}$$

Let

$$Z = \frac{1}{K_1\sigma_1}Y_{K_1} - \frac{1}{K_0\sigma_0}Y_{K_0}, \tag{21}$$

$$\Delta_1 = 6\sqrt{2\pi}\ln(N - p_{\max})(K_0 - K_1), \tag{22}$$

$$\Delta_2 = 2N\left(\frac{1}{K_1\sigma_1} - \frac{1}{K_0\sigma_0}\right), \tag{23}$$

$$\Delta = \Delta_1 + \Delta_2. \tag{24}$$

Equation (20) becomes

$$P_{\text{error}} = P\{Z < \Delta\}. \tag{25}$$

From statistical knowledge, probability density function of random varible Z is

$$\mathrm{f}_Z(z) = \begin{cases} C\exp[(K_0\sigma_0/2)z]\left[\sum\limits_{l=0}^{m_0}\left(\begin{array}{c} m_0 \\ l \end{array}\right)\frac{(m_0+m_1-l)!}{a^{m_0+m_1-l+1}}(-z)^l\right] & (z<0) \\ C\exp[(K_1\sigma_1/2)z]\left[\sum\limits_{l=0}^{m_0}\left(\begin{array}{c} m_0 \\ l \end{array}\right)\frac{(m_0+m_1-l)!}{a^{m_0+m_1-l+1}}(z)^l\right] & (z\geqslant 0) \end{cases}, \tag{26}$$

where

$$\left(\begin{array}{c} m_0 \\ l \end{array}\right) = \frac{m_0!}{l!(m_0-l)!}, \tag{27}$$

$$m_0 = \frac{N - K_0 + \sum\limits_{j=1}^{K_0} p_j}{2} - 1 \quad \text{or} \quad m_1 = \frac{N - K_1 + \sum\limits_{j=1}^{K_1} p_j}{2} - 1, \tag{28}$$

$$a = \frac{K_0\sigma_0 + K_1\sigma_1}{2}, \tag{29}$$

$$C = \frac{1}{m_0!m_1}\left(\frac{K_0\sigma_0}{2}\right)^{m_0+1}\left(\frac{K_1\sigma_1}{2}\right)^{m_1+1}, \tag{30}$$

and

$$P_{\text{over}} = \sum_{l=0}^{m_0}\left(\begin{array}{c} m_1+m_0-l \\ m_1 \end{array}\right)\frac{\gamma^{m_1-m_0+l+1}e_0}{(\gamma+\gamma^{-1})^{m_1+m_0-l+1}}(\Delta<0), \tag{31}$$

$$P_{\text{under}} = \begin{cases} \sum\limits_{l=0}^{m_0}\left(\begin{array}{c} m_1+m_0-l \\ m_1 \end{array}\right)\frac{\gamma^{m_1-m_0+l+1}e_0}{(\gamma+\gamma^{-1})^{m_1+m_0-l+1}} & (\Delta<0) \\ \sum\limits_{l=0}^{m_0}\left(\begin{array}{c} m_0+m_1-l \\ m_1 \end{array}\right)\frac{\gamma^{m_1-m_0+l+1}(1+\gamma^{-2l-2}(1-e_1))}{(\gamma+\gamma^{-1})^{m_1+m_0-l+1}} & (\Delta\geqslant 0) \end{cases}, \tag{32}$$

where

$$\gamma = \sqrt{\frac{K_1\sigma_1}{K_0\sigma_0}}, \tag{33}$$

$$e_0 = \sum_{j=0}^{l}\frac{\left(-\frac{K_0\sigma_0}{2}\Delta\right)^j}{j!}\exp[(K_0\sigma_0/2)\Delta], \tag{34}$$

$$e_1 = \sum_{j=0}^{l}\frac{\left(\frac{K_1\sigma_1}{2}\Delta\right)^j}{j!}\exp[-(K_1\sigma_1/2)\Delta]. \tag{35}$$

After the number of SAR image regions is detected and the MMAR model parameters are estimated, SAR image segmentation is performed by classifying pixels. In some case, the Bayesian classifier is used for implementing classification. That is, if

$$\pi_{k_0}\Phi\left[\frac{e_{k_0}(s)}{\sigma_{k_0}}\right] > \pi_k\Phi\left[\frac{e_k(s)}{\sigma_k}\right], \quad (k = 1, 2, \cdots, K, k \neq k_0), \tag{36}$$

then

$$X(s) \in \mathbf{G}_{k_0}. \tag{37}$$

Suppose an image is segmented into K image regions, denoted by $\mathbf{G}_1, \cdots, \mathbf{G}_K$. Then given that the true image region is $\mathbf{G}_{k_0}$, the probability of misclassification is

$$P_{\text{mis}}(\bullet|\mathbf{G}_{k_0}) = \pi_{k_0}\sum_{k=1,k\neq k_0}^{K}\int_{\mathbf{G}_k}\mathrm{d}\Phi\left(\frac{e_{k,s}^2}{\sigma_k}\right). \tag{38}$$

To demonstrate the segmentation performance of our proposed algorithm, in this section we present three examples of unsupervised segmentation of complex SAR images, which are size of 128×128 pixel resolution, consisting of forest and grass (or cornfield) in Fig. 2(a). From the complex images, we generate an abovementioned quadtree representation consisting of $L = 7$ levels and use a third-order regression. Because it is found that by increasing the regression order to $p = 3$ for both grass and forest, we can achieve a lower probability of misclassification and a good trade-off between modeling accuracy and computational efficiency. We randomly select 1200 representative pixels from the original images. The detection of the number of SAR image regions is given. The BSAEM algorithm is then used for parameters estimation. In these detection and estima-

tion, there are 200 repetitions. We compute the average value of all the estimates. Then, Bayesian classification is adopted for pixels classification.

Table 1 summarizes the detection results. It shows that the number of SAR image regions indicated by the BIC criterion is correct for three SAR images, that is, $K_1 = 2$ is equal to the correct number of image regions, $K_0 = 2$. Probabilities of over-detecting and under-detecting the number of SAR image regions are almost zero.

Figure 2(d) show segmentation results based on BSAEM algorithm for the MMAR model, as well as results (see Figs. 2(b) and (c)) based on the mixture Gaussian model (MGM) on the single resolution and the MMAR model using EM algorithm, respectively. Table 2 shows the misclassification probability of pixel classified by BSAEM algorithm, EM algorithm and MGM for the three SAR images. And Table 3 shows the time of segmentation images under P4 computer. From Fig. 2 and Table 2, the segmentation results based on the MMAR model are better then that based on the MGM, while, BSAEM algorithm and EM algorithm perform similarly. However, Table 3 shows that BSAEM algorithm considerably reduces the segmentation time.

Figure 3 illustrates the convergence of EM and BSAEM with a plot of increment of training set log-likelihood over the 125 iterations of the algorithm. The increment of data likelihood is minimal after about 20 iterations, and

Table 1. Detection Results of SAR Images in Fig. 2(a) (K_0=2)

	BIC				K_1	P_{under}	P_{over}
	$K=1$	$K=2$	$K=3$	$K=4$			
Fig. 2(a) (top)	33 682	21 059	24 217	36 526	2	0	0
Fig. 2(a) (middle)	19 865	13 682	16 049	26 118	2	0	0
Fig. 2(a) (below)	30 157	17 286	17 419	24 589	2	0	1.58×10^{-6}

Table 2. Misclassification Probabilities for Images in Fig.2(a)

	P_{mis}(.|forest)			P_{mis}(.|grass)		
	MGM	MMAR		MGM	MMAR	
		EM	BSAEM		EM	BSAEM
Fig. 2(a)(top)	4.290	2.719	4.467	6.361	1.618	1.369
Fig. 2(a)(middle)	20.82	3.028	1.892	10.283	0.9273	0.8184
Fig. 2(a)(below)	2.570	2.776	3.162	8.57	1.527	1.619

Table 3. Time of Segmentation under P4(2.3) Computer(s)

	MGM	MMAR	
		EM	BSAEM
Fig. 2(a)(top)	194	2 637	470
Fig. 2(a)(middle)	328	4 324	793
Fig. 2(a)(below)	316	2 427	736

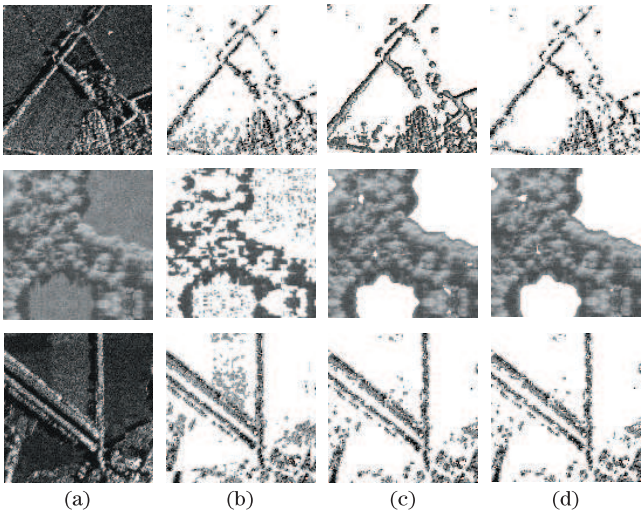

Fig. 2. (a) Original SAR images; (b) segmented images based on MGM; (c) segmented images from EM algorithm based on the MMAR; (d) segmented images from BSAEM algorithm based on the MMAR.

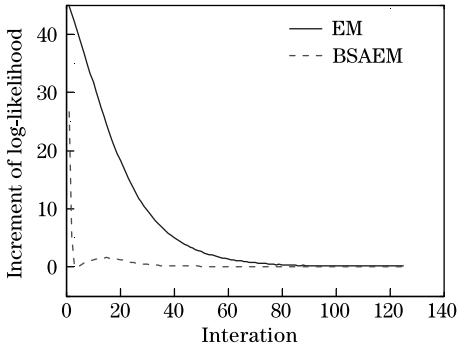

Fig. 3. Convergence of EM and BSAEM algorithm.

convergence occurs at around 55 iterations. But, the increment of data likelihood is minimal after about 80 iterations, and convergence occurs at around 110 iterations.

By using Bootstrap technique, an unsupervised Bayesian segmentation and its performance evaluation can be achieved based on the MMAR model. The proposed algorithm allows an estimation of parameters of MMAR model of SAR image from a small-sized sample with regard to that of the initial sample of observations. As a result, the interest in the analysis of the images is based on the gain in times of calculation. Experiments demonstrated that for the segmentation techniques of SAR image, the detection procedure is robust, the parameter estimates are accurate, and the results are in good agreement.

This work was supported by the National High Technology Research and Development Program of China (No. 2010AA122201) and the National Natural Science Foundation of China (Nos. 61102125 and 60872064).

References

1. P. K. Sahoo, S. Soltani, A. K. C. Wong, and Y. C. Chen, Comput. Vis. Graph. Image Process. **41,** 233 (1988).

2. J. S. Weszka, Comput. Vis. Graph. Image. Process. **7,** 259 (1978).
3. D. A. Clausi, Pattern Recogn. **35,** 1959 (2002).
4. A. K. Jain, R. P. W. Duin, and J. Mao, IEEE Trans. Pattern Anal. Mach. Intell. **22,** 4 (2000).
5. J. Gambini, M. E. Mejail, J. Jacobo-Berlles, and A. C. Frery, Stat. Comput. **18,** 15 (2008).
6. S. A. Hojjatoleslami and J. Kittler, IEEE Trans. Image Process. **7,** 1079 (1998).
7. M. S. Allili and D. Ziou, Pattern Recogn. Lett. **28,** 1946 (2007).
8. C. Bouman and B. Liu, IEEE Trans. Pattern Anal. Mach. Intell. **13,** 99 (1991).
9. C. A. Bouman and M. Shapiro, IEEE Trans. Image Process. **3,** 162 (1994).
10. M. Mignotte, C. Collet, P. Pérez, and P. Bouthemy, IEEE Trans. Image Process. **9,** 1216 (2000).
11. C. H. Fosgate, W. W. Irving, W. C. Karl, and A. S. Willsky, IEEE Trans. Image Process. **6,** 7 (1997).
12. W. W. Irving, L. M. Novak, and A. S. Willsky, IEEE Trans. Aero. Electron. Syst. **33,** 1157 (1997).
13. A. Kim and H. Krim, IEEE Trans. Signal Process. **47,** 458 (1999).
14. M. Basseville, A. Benveniste, and A. S. Willsky, IEEE Trans. Signal Process. **40,** 1915 (1992).
15. M. Basseville, A. Benveniste, and A. S. Willsky, IEEE Trans. Signal Process. **40,** 1935 (1992).
16. A. Alonso-González, C. López-Martínez, and P. Salembier, in *Proceedings of 2010 IEEE International Geoscience and Remote Sensing Symposium* 4043 (2010).
17. M. L. Comer and E. J. Delp, IEEE Trans. Image Process. **8,** 408 (1999).
18. X. B. Wen and Z. Tian, Electron. Lett. **39,** 1272 (2003).
19. B. Efron, Ann. Stat. **7,** 1 (1979).